# Development of the ALMA Band-3 and Band-6 Sideband-Separating SIS Mixers

Anthony R. Kerr, *Life Fellow, IEEE*, Shing-Kuo Pan, *Member, IEEE*, Stéphane M. X. Claude, Philip Dindo, Arthur W. Lichtenberger, John E. Effland, *Member, IEEE*, and Eugene F. Lauria, *Member, IEEE*

***Abstract*—As the Atacama Large Millimeter/submillimeter Array (ALMA) nears completion, 73 dual-polarization receivers have been delivered for each of Bands 3 (84–116 GHz) and 6 (211–275 GHz). The receivers use sideband-separating superconducting Nb/Al-AlOx/Nb tunnel-junction (SIS) mixers, developed for ALMA to suppress atmospheric noise in the image band. The mixers were designed taking into account dynamic range, input return loss, and signal-to-image conversion (which can be significant in SIS mixers). Typical SSB receiver noise temperatures in Bands 3 and 6 are 30 and 60 K, respectively, and the image rejection is typically 15 dB.**

***Index Terms*—Atacama Large Millimeter/submillimeter Array (ALMA), heterodyne, image rejecting mixer, interferometer, millimeter-wave, radio astronomy, sideband-separating mixer, SIS junction, SIS receiver, superconductor.**

## I. Introduction

THE superconducting tunnel diode, specifically the superconductor–insulator–superconductor (SIS) junction, is now the preferred mixing element for low-noise heterodyne receivers at millimeter and submillimeter wavelengths. Since the introduction of the SIS mixer in 1979 [1]–[3], it has evolved from a delicate, short-lived, Pb-alloy device, difficult to fabricate reproducibly and marginally suitable for field operation, to today's relatively robust and reproducible device, usually with Nb/Al-AlOx/Nb tunnel junctions. Early SIS mixers had SIS junctions suspended across a waveguide and one or more mechanical tuners to tune out the relatively large junction capacitance [4], a configuration with limited instantaneous bandwidth and far from suitable for operation in large numbers and at remote sites as required for the Atacama Large Millimeter/submillimeter Array (ALMA) [5]. The adaptation of thin-film processing techniques from the semiconductor industry for use with Nb-based circuits has made possible the integration of tuning circuits with the SIS junctions to yield relatively wideband operation, typically 1.3:1 RF bandwidth and ∼ 8-GHz IF bandwidth, without mechanical tuners [6]–[8].

Before ALMA, SIS receivers operated in the simple double-sideband mode, responding to signals in both upper and lower sidebands. For spectral-line radio astronomy, which is a major focus of ALMA, atmospheric noise entering a DSB receiver in the unwanted image sideband adds substantially to the overall system noise, thereby degrading the sensitivity of the measurement. In addition, for single-dish (as opposed to interferometric) observations, spectral lines from the unwanted sideband appear at IF and can greatly complicate the identification of molecules from their emission spectra. For these reasons, the North American ALMA receivers use sideband-separating SIS mixers. Sideband separation can be achieved in several ways in heterodyne receivers. An input diplexer can be used to couple the upper and lower sidebands into separate double-sideband mixers. At millimeter and submillimeter wavelengths, mechanically tuned quasioptical diplexers such as the Mach–Zehnder and Martin–Puplett interferometers have been used [9]–[11]. However, these have insufficient bandwidth [12] to operate with ALMA's octave or wider IF bands. For the ALMA Band-3 (84–116 GHz) and Band-6 (211–275 GHz) receivers the phasing type of sideband-separating mixer is used [13], as depicted in Fig. 1. A pair of elemental DSB mixers, driven by a common LO source, are connected by quadrature hybrids to the RF source and IF load. Because the two elemental mixers do not interact, an optimized DSB mixer is also optimal for use in the sideband-separating receiver.

An early design integrating the elements of a complete 200–300-GHz sideband-separating SIS mixer (RF quadrature hybrid, LO couplers, and two DSB SIS mixers with RF tuning circuits) on a single chip was largely successful [13], [14]. However, the large size of the chips would have required many wafers to be produced, with significantly higher cost than a waveguide-based circuit incorporating a pair of much smaller chips, each containing a single DSB SIS mixer with its RF tuning circuit and a waveguide coupling probe [15].

## II. Design of the Elemental SIS DSB Mixers

### A. SIS Junctions

The quantum theory of SIS mixers, published in 1983 and 1985 by Tucker and Feldman [16], [17], has been the basis for

Manuscript received November 03, 2013; revised December 15, 2013; accepted January 16, 2014. Date of publication February 13, 2014; date of current version March 04, 2014. This work was supported in part by the National Radio Astronomy Observatory.

A. R. Kerr, S.-K. Pan, and J. E. Effland are with the National Radio Astronomy Observatory, Charlottesville, VA 22903 USA (e-mail: akerr@nrao.edu; span2@nrao.edu; jeffland@nrao.edu).

S. M. X. Claude and P. Dindo are with the National Research Council—Herzberg, Victoria, BC V9E 2E7 Canada (e-mail: Stephane.Claude@nrc-cnrc.gc.ca; Philip.Dindo@hotmail.com).

A. W. Lichtenberger is with the University of Virginia, Charlottesville, VA 22904 USA (e-mail: awl1l@virginia.edu).

E. F. Lauria is with the University of Arizona, Tucson, AZ 85721 USA (e-mail: glauria@email.arizona.edu).

Color versions of one or more of the figures in this paper are available online at http://ieeexplore.ieee.org.

Digital Object Identifier 10.1109/TTHZ.2014.2302537

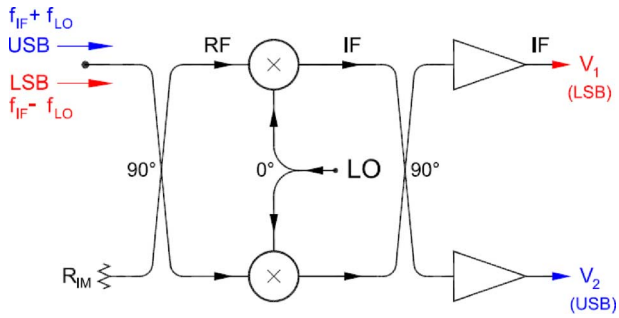


Fig. 1. Phasing type of sideband-separating mixer, as used in Band-3 and -6 ALMA SIS receivers, uses two elemental DSB mixers.

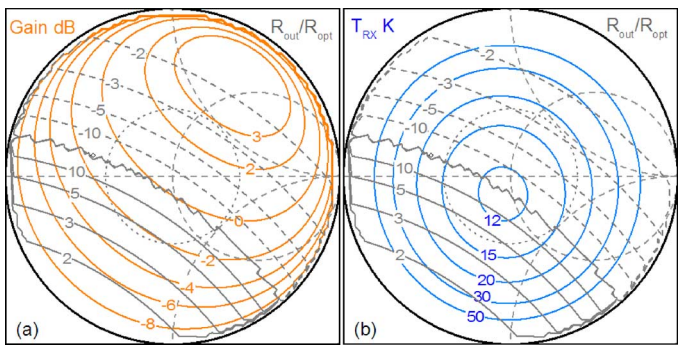


Fig. 2. For the elemental DSB Band-3 SIS mixer with $f_{\rm LO} = 100$ GHz, contours of (a) mixer gain dB (solid orange lines) and (b) noise temperature (solid blue lines) plotted on a Smith chart of the RF source impedance normalized to the optimum source impedance $R_{\rm opt}$. The gray contours are the IF output resistance of the mixer normalized to $R_{\rm opt}$; solid gray lines indicate positive output resistance and dashed gray lines indicate negative output resistance. The squiggly gray line indicates the transition from positive to negative output resistance. The dashed gray circle at $|\rho| = 0.4$ indicates the boundary of the desirable operating region [20]. The simulations used the $I(V)$ curve of Fig. 6. A 4-K IF isolator of characteristic impedance $R_{\rm opt}$, and an amplifier noise temperature of 4 K were assumed.

all subsequent SIS mixer design. The noise and conversion characteristics of an SIS mixer depend on the embedding impedance seen by the junction at the sideband frequencies $nf_{\rm LO} \pm f_{\rm IF}$ and at the LO harmonics $nf_{\rm LO}$. Under typical operating conditions, for an SIS junction with normal resistance $R_{\rm N}$, an optimum RF source impedance, based on the Tucker theory, is given by the Ke and Feldman formula [18]

$$R_{\rm opt} = 4R_{\rm N}\left(2 + \frac{eV_{\rm g}}{hf_{\rm LO}}\right)^{-1}$$

where $eV_{\rm g}$ is the superconducting energy gap, $h$ is Planck's constant, and $f_{\rm LO}$ is the local oscillator frequency. This formula applies to mixers with a single junction or a series array of junctions; in both cases, $eV_{\rm g}$ is the superconducting energy gap of a single junction. The simulated results in Figs. 2–5 show how the characteristics of the elemental DSB mixers for ALMA Bands 3 and 6 depend on the RF source impedance for representative LO frequencies 100 and 230 GHz, respectively. Fig. 2(a) shows contours of gain in dB (heavy orange lines) and IF output impedance normalized to $R_{\rm opt}$ (gray lines, dashed where the output resistance is negative) for the Band-3 mixer biased near the middle of the first photon step and with the LO

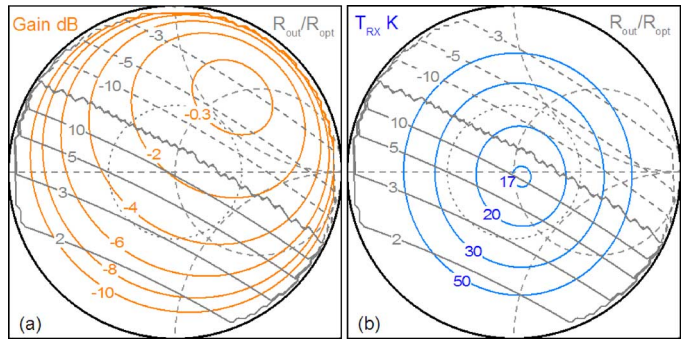


Fig. 3. For the elemental DSB Band-6 SIS mixer with $f_{\rm LO} = 230$ GHz. The simulations used the $I(V)$ curve of Fig. 7. Details are the same as for Fig. 2.

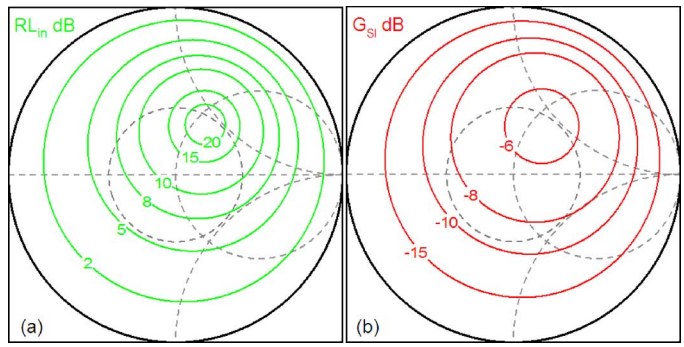


Fig. 4. For the elemental DSB Band-3 SIS mixer with $f_{\rm LO} = 100$ GHz, contours of (a) RF input return loss in dB (solid green lines) and (b) signal-to-image conversion gain in dB (solid red lines), plotted on a Smith chart of the RF source impedance normalized to the optimum source impedance $R_{\rm opt}$. The dashed gray circles at $|\rho| = 0.4$ indicate the boundary of the desirable operating region [20]. A 4-K IF isolator of characteristic impedance $R_{\rm opt}$ is assumed in these simulations.

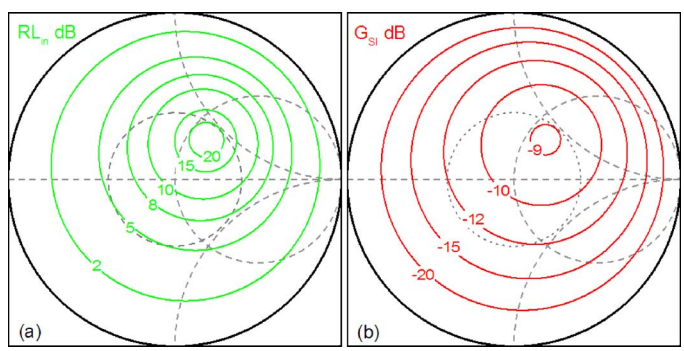


Fig. 5. For the elemental DSB Band-6 SIS mixer with $f_{\rm LO} = 230$ GHz.. Details are the same as for Fig. 4.

power adjusted for a pumping parameter $\alpha = eV_{\rm LO}/hf = 1.2$. Fig. 2(b) shows contours of receiver noise temperature $T_{\rm Rx}$. Fig. 3(a) and (b) shows the same for the Band-6 mixer. Figs. 4 and 5 show the corresponding contours of RF input return loss and signal-to-image conversion gain for the elemental Band-3 and -6 DSB mixers. The contours in Figs. 2–5 are plotted on Smith charts of the RF source impedance (which includes the junction capacitance) normalized to $R_{\rm opt}$. The gain is the transducer gain, with the mixer terminated in an IF isolator of characteristic impedance equal to $R_{\rm opt}$ for the reasons given below.

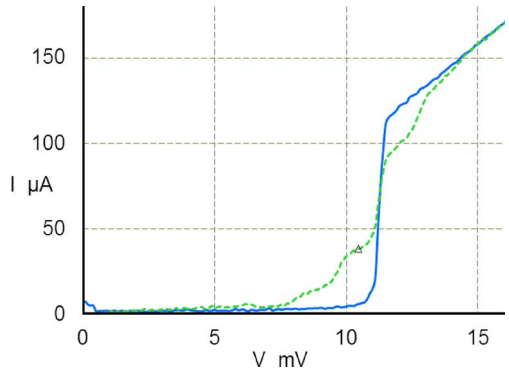


Fig. 6. Pumped and unpumped $I(V)$ curves of a typical four-junction SIS mixer for Band 3. The operating bias point is indicated by the marker. The quality factor $R(8\ \mathrm{mV})/R_{\mathrm{N}} = 31$, and the pumping parameter $\alpha \approx 1.2$.

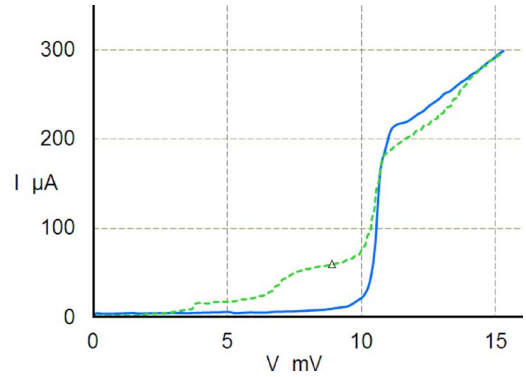


Fig. 7. Pumped and unpumped $I(V)$ curves of a typical four-junction SIS mixer for Band-6. The operating bias point is indicated by the marker. The quality factor $R(8\ \mathrm{mV})/R_{\mathrm{N}} = 21$, and the pumping parameter $\alpha \approx 1.2$.

The receiver noise temperatures are the single-sideband quantities [19] for the DSB mixer with the isolator at 4 K and an IF amplifier noise temperature of 4 K.

It is evident in Figs. 2 and 3 that the output impedance of the SIS mixers is negative when the source impedance lies in much of the upper half of the Smith chart and that the maximum conversion gain occurs in the region of negative output resistance. Negative resistance and $\mathrm{gain} > 1$ are a result of the nonclassical nature of the SIS mixer and are not parametric effects—unlike a semiconductor diode, the capacitance of an SIS junction is not voltage-dependent. The implications of negative output resistance in designing SIS mixer circuits are discussed in [20]. To optimize the overall receiver noise, it can be appropriate to operate an SIS mixer in the region of high output resistance, positive or negative. To avoid a large RF input mismatch, and even negative RF input resistance, the IF load impedance should not be large relative to $R_{\mathrm{opt}}$. We have found that an IF load equal to the optimum RF source resistance $R_{\mathrm{opt}}$ is a good compromise. This also results in acceptable signal-to-image conversion. The signal-to-image conversion gain $G_{\mathrm{SI}}$ of the elemental DSB mixers, as shown in Figs. 4(b) and 5(b), is particularly important to consider in sideband-separating receivers. Signal power converted to the image frequency can be partially reflected by any mismatched components in the input circuit, such as an imperfect OMT or feed horn, and appear at IF as a spurious image frequency signal, thereby degrading the image rejection.

The simulations used the $I(V)$ characteristics of the Band-3 and -6 production mixers, shown in Figs. 6 and 7. The LO voltage waveform is assumed to be sinusoidal; this is a good approximation [21] for SIS junctions which, by virtue of their parallel-plate construction, have a relatively large shunt capacitance. The embedding impedances seen by the SIS junctions at the higher harmonic sideband frequencies also affect mixer performance, and it is assumed here that the junctions are terminated in their own capacitance at the second-harmonic sideband frequencies $2f_{\mathrm{LO}} \pm f_{\mathrm{IF}}$ and short-circuited by their own capacitance at higher frequencies—this is the *quasi-five frequency* approximation [21] which has been found to give reasonably accurate results.

The mixers for Bands 3 and 6 use series arrays of four SIS junctions with an optimum source resistance near 50 Ω, which is a convenient impedance level for coupling to the waveguide probe and allows direct connection to a 50-Ω IF stage. The use of a series array of $N$ junctions in an SIS mixer has two advantages compared with a single junction. For the same overall impedance level, the individual junctions of the array are larger, which makes them easier to fabricate consistently. Also, the dynamic range (or saturation power) of an SIS mixer, which depends on $N^2 f^2$ [22], [23], is greater; this is particularly important for the ALMA receivers which are required to have less than 5% gain compression when connected to a 373-K calibration source. It was shown theoretically by Feldman and Rudner [24] that the noise of an SIS mixer with $N$ junctions in series is the same as that of a single-junction mixer with the same impedance level as the array, i.e., for the same critical current density, the junctions in the array have $N$ times the area of the single junction. The array requires $N^2$ times the LO power, but that is not a significant limitation for current single-pixel SIS receivers.

The mixing properties of an SIS junction are largely defined by its normal resistance $R_{\mathrm{N}}$, which depends on the junction area $A$ and critical current density $J_C$ [25], and by the junction capacitance $C_J$. For the Nb/Al-AlOx/Nb junctions used in this work, $R_{\mathrm{N}}A = 1.8 \times 10^{-3}/J_C$, and the specific junction capacitance $C_{\mathrm{S}}$ is given by the empirical expression [26]

$$C_{\mathrm{S}} = 24.9 \log_{10}\left(J_C\ (\mathrm{A/cm^2})\right) - 18.1\ \ \mathrm{fF}/\mu\mathrm{m}^2.$$

The choice of junction area and critical current density to give the desired $R_{\mathrm{N}}$ requires a compromise between junction quality and reproducibility on the one hand versus junction capacitance on the other. A small junction with low capacitance will have wider RF bandwidth but requires a higher value of $J_C$ (for the desired $R_{\mathrm{N}}$) which results in an $I(V)$ characteristic with greater leakage current and therefore higher shot noise. For the ALMA Band-3 mixers, the nominal junction diameter is 2.2 $\mu$m, $J_C = 2\,,500$ A/cm$^2$, $R_{\mathrm{N}} = 76\ \Omega$, and $C_{\mathrm{S}} = 67$ fF/$\mu$m$^2$, and for Band 6 the junction diameter is 1.7 $\mu$m, $J_C = 5\,,200$ A/cm$^2$, $R_{\mathrm{N}} = 61\ \Omega$, and $C_{\mathrm{S}} = 74$ fF/$\mu$m$^2$. (The $R_{\mathrm{N}}$ values are for the four junctions in series.)

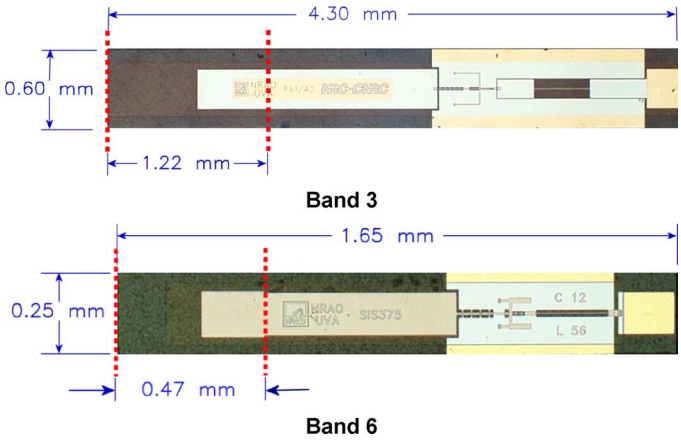


Fig. 8. Photographs of the Band-3 and -6 mixer chips (different scales). Dark areas are the background seen through the quartz substrate. The suspended stripline waveguide probe (to the left) connects through a broadband transition to a capacitively loaded CPW. The dc/IF bonding pad is at the right. The dotted red lines indicate the position of the broad-walls of the waveguide. Figs. 9 and 10 show more details.

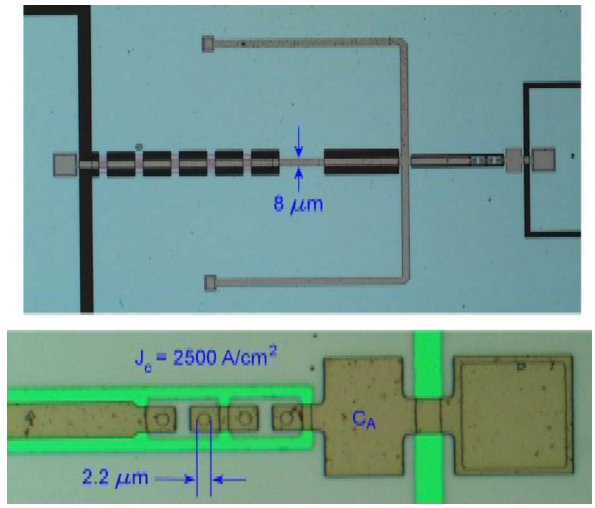


Fig. 9. RF circuit of the Band-3 SIS mixer chip [8]. Dark or green regions are the background seen through the quartz substrate and contain no metallization. The lower Nb base-electrode metallization is light gray; the darker (brown) conductors are the Nb wiring layer.

### B. Circuit Design of the Elemental DSB Mixer Chips

Substrate materials compatible with the niobium SIS mixer fabrication process are silicon ($\varepsilon_r = 12$) and fused quartz ($\varepsilon_r = 3.8$). A fused quartz substrate was chosen for its relatively low dielectric constant which allows a wider substrate to be used without the possibility of exciting higher modes in the substrate channel. The mixer chips were fabricated on 50-mm-diameter wafers at the University of Virginia Microfabrication Laboratory between 2003 and 2008 using their then standard Nb/Al-Ox/Nb trilayer junction process [27].

The mixer circuit is coupled to a full-height input waveguide by a rectangular suspended-stripline probe with a return loss $>$ 21 dB over the full waveguide band [28]. Photographs of the Band-3 and -6 mixer chips are shown in Fig. 8. The suspended stripline waveguide probe (at the left) is connected to the mixer circuit through a broadband transition to capacitively loaded coplanar waveguide [13], a CPW with periodic capacitive loading by ground bridges to give a characteristic impedance of 50 ohms on the quartz substrate while suppressing slot modes in the ground plane. The Nb ground plane and wiring layer are on the same side of the quartz substrate, separated by a 285-nm SiOx dielectric layer with $\varepsilon_r = 4.2$. To achieve the range of characteristic impedances required for the RF matching circuit with this thin dielectric layer without requiring impractical dimensional tolerances, CPW is used for higher impedance ($\sim 90\ \Omega$) sections and microstrip is used for lower impedances ($\sim 7\ \Omega$); capacitively loaded CPW is used for intermediate impedance values. A thicker 570-nm SiOx layer is used under the CPW loading capacitors.

To maximize the RF coupling bandwidth between a resistive source and a series array of capacitive devices, such as SIS junctions, the series inductance of the array must be optimized as described in [20]. If the array inductance is small it may be desirable to increase it, as in the case of the Band-3 mixer described here, but too large an array inductance can severely limit the bandwidth.

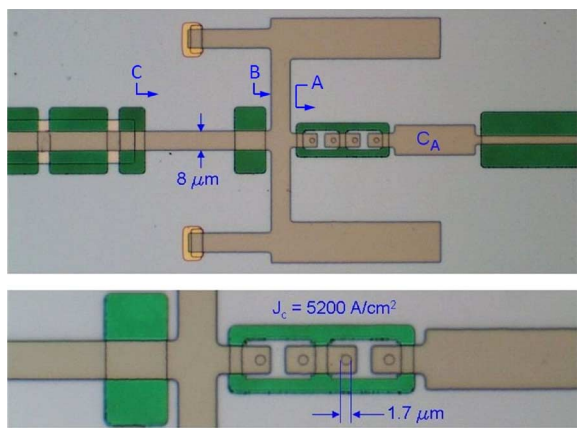


Fig. 10. RF circuit of the Band-6 SIS mixer chip [38]. Dark or green regions are the background seen through the quartz substrate and contain no metallization. The lower Nb base-electrode metallization is light gray; the darker (brown) conductors are the Nb wiring layer.

A wide IF bandwidth requires the inductance in the IF circuit of the mixer to be minimized. This is achieved using the configuration described in [7] in which the IF current bypasses the waveguide coupling circuit.

The on-chip RF circuits of the Band-3 and -6 mixers are similar, as shown in Figs. 9 and 10. At the left is the capacitively loaded CPW line from the suspended stripline waveguide probe, connected to a parallel pair of broadbanding resonators, the series array of four SIS junctions, a tuning capacitor $C_A$, and, at the right, the end of the RF choke. For Band 3, the two resonators are quarter-wave microstrip short-circuit stubs, and for Band 6 each resonator consists of a short inductive microstrip stub connected in parallel with a short capacitive stub, which approximates a parallel $LC$ resonator connected at the input of the SIS array. For both mixers, the resonators are tuned near the middle of the RF band to give the desired frequency response.

For brevity, only the operation of the Band-6 circuit will be described in detail here. The equivalent circuit of the mixer chip

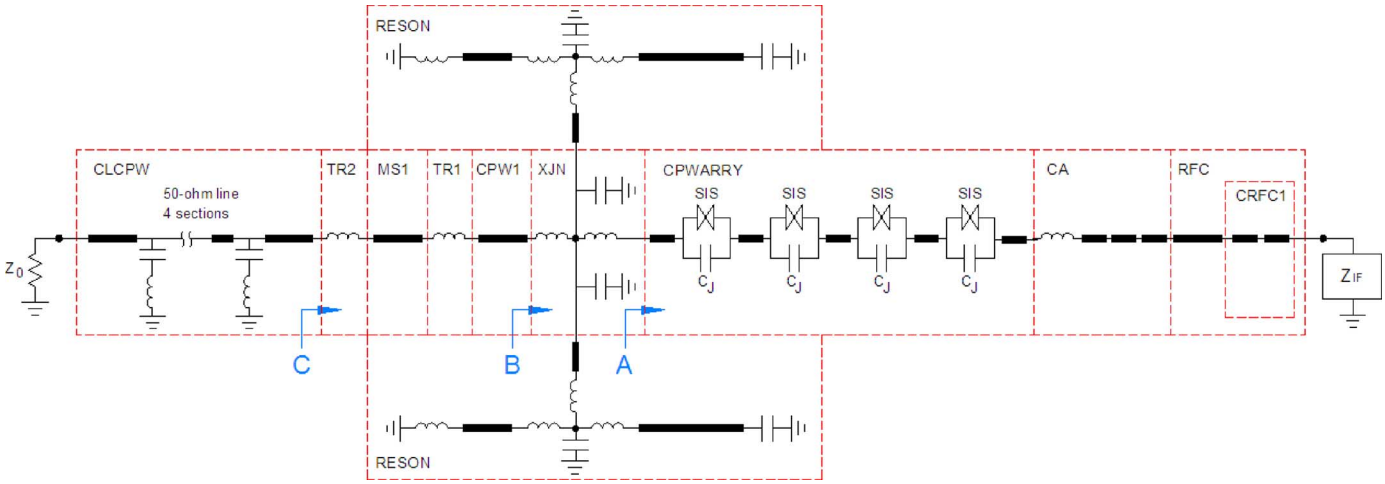


Fig. 11. Equivalent circuit of the Band-3 and -6 SIS mixers. At the left, the circuit connects to the suspended stripline waveguide probe. The two broadbanding resonators are at the top and bottom of the diagram (resonator details are for Band 6). The IF and dc connection is at the right. Locations A, B, and C correspond to those shown in Fig. 10. CLCPW is the capacitively loaded CPW input line; TR2 and TR1 represent fringing inductances at the transitions between elements; MS1 is a microstrip line; CPW1 a CPW line; XJN is the junction of CPW1, the two resonators RESON, and the series array CPWARRAY of four SIS junctions; $C_A$ is a short section of low-impedance microstrip; and RFC is the RF choke in the IF/dc circuit.

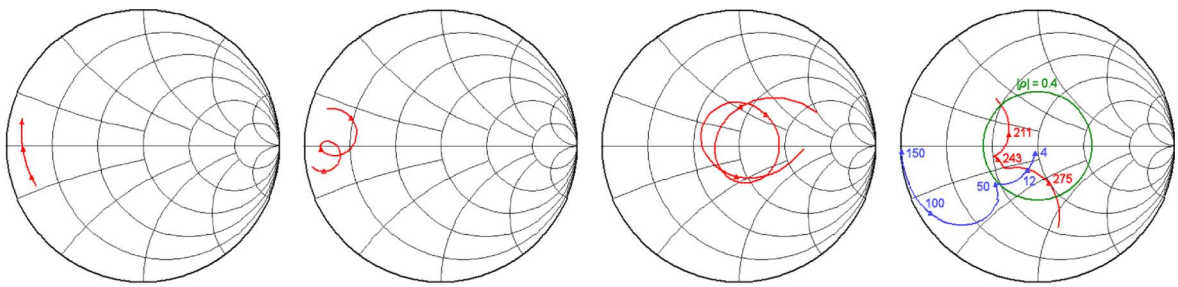


Fig. 12. Smith chart plots of the impedance at various points through the circuit of Fig. 11. (a)–(c) Reflection coefficients looking to the right at planes A, B, and C, respectively, normalized to $Z_0 = 50\ \Omega$, over 200–280 GHz. (d) Reflection coefficient seen by the SIS junctions over the same RF band (red), and from 4 to 150 GHz (blue), normalized to $R_{opt}$. The circle $|\rho| = 0.4$ (green) is included for [20].

is shown in Fig. 11. The different sections outlined by the dashed boxes were individually modeled using Sonnet *em* [29]. Because the conductors on the chip are all superconducting Nb, they can be considered lossless, but they have a frequency-independent surface inductance due to the London penetration depth (similar to the skin depth in normal conductors) which is included explicitly in the Sonnet simulations. The surface inductance is not of consequence in the CPW sections, but it must be taken into account in the microstrip sections in which the dielectric thickness is not much greater than the penetration depth ($\sim$ 85 nm in Nb). The appropriate value of surface inductance for thick and thin superconducting transmission lines is discussed in [30]. The elements in Fig. 11 were optimized using the microwave circuit simulator MMICADv2 [31]. Fig. 12(a)–(c) shows the impedance looking into the array of SIS junctions from locations A, B, and C, as indicated in Figs. 10 and 11, when the SIS junctions have an impedance equal to their optimum source impedance. The embedding impedance $Z_e$ seen by the four junctions is shown in Fig. 12(d). Over the RF band, $Z_e$ lies well within the desirable region $|\rho| \leq 0.4$. (In fact, $Z_e$ is slightly different for each of the four junctions but the differences are too small to see in this diagram.) The concept of embedding impedance needs some clarification for the case of multiple SIS junctions. It is the impedance which would be seen by a test signal source connected in place of one of the junctions when identical sources are connected in place of the other junctions. Also shown in Fig. 12(d) is the impedance seen by the junctions over the IF band, extended to 150 GHz, with the IF port of the mixer substrate terminated in $Z_{IF} = 50\ \Omega$. It is evident that the impedance is well behaved and less than 50 Ω over the extended IF band. This is important for maintaining stability of the mixer as explained in [20]. (The acceptable behavior of the embedding impedance over this extended IF band, with the mixer chip terminated in 50 Ω, ensures only that the chip itself is free of undesired characteristics. The structure between the chip and the IF amplifier is substantially overmoded at 150 GHz and in principle could introduce undesired resonances in the upper part of the extended IF band, although this appears not to be significant in the present design.)

### C. IF Inter-Stage Network

The IF output of the Band-3 mixer chip is connected by a pair of bond wires to a 50-Ω SMA connector and then by a cable to

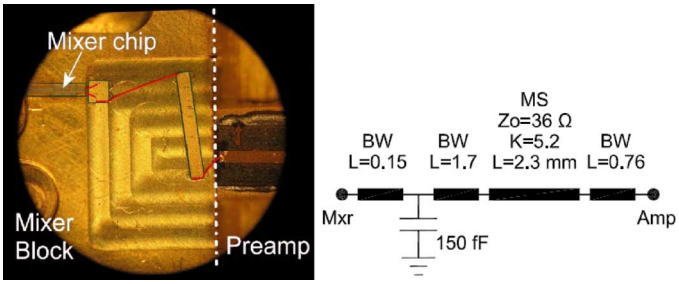


Fig. 13. Details of the IF interstage network used in the Band-6 mixer. BW = bond-wire (red), MS = microstrip. Lengths L are in mm.

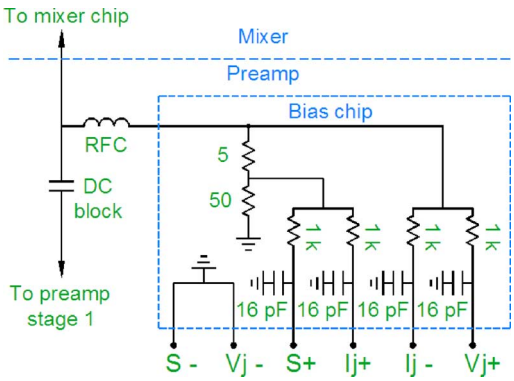


Fig. 14. Details of the SIS mixer bias circuit. The 5-Ω resistor monitors the mixer current, and the 1-k resistors and 16-pF capacitors provide ESD protection.

the IF isolator and amplifier. For the Band-6 mixer, no IF isolator is used and a simple phasing network between the mixer chip and the preamplifier input allows the mixer-preamp performance to be optimized for RF input match, signal-to-image conversion, and gain flatness within the IF band. Fig. 13 shows the details of the interstage network.

### D. Mixer Bias Circuit

The ALMA SIS mixers use a six-wire bias circuit based on the one described in [32], as shown in Fig. 14. The bias voltage for the mixer is developed across the 50-Ω resistor by a current source connected to $S^+$ and $S^-$, and the junction current is monitored by the 5-Ω resistor at $I_j^+ - I_j^-$. A servo loop controls the current source to maintain a constant bias voltage at the mixer ($V_j^+ - V_j^-$). The presence of the 50-Ω resistor ensures that the bias circuit has a low impedance from dc to well beyond the bandwidth of the servo loop, which is desirable for maintaining the stability of the bias circuit.

For both Bands 3 and 6, the bias circuit is built into the IF preamplifier and connects to the mixers through the IF circuit, and in the case of Band 3, through the IF isolator whose center conductor is isolated from ground [33]. For Band 3, the bias circuit uses discrete components and for Band 6 it is on a custom silicon chip [34].

### E. Magnetic Circuit

Conduction in SIS junctions is by two types of carrier, superconducting Cooper pairs (of electrons), and quasi-particles

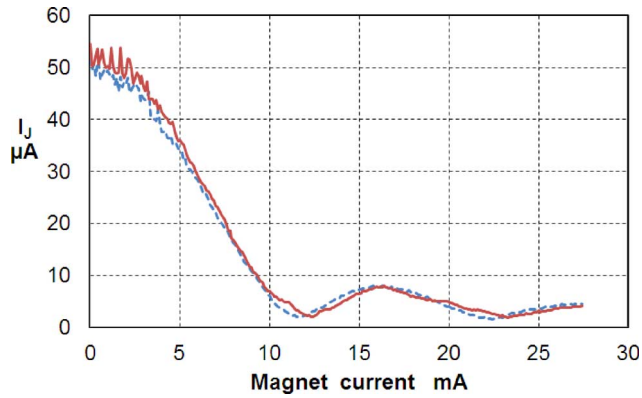


Fig. 15. Plot of critical current versus magnet current for the two mixer chips in a typical Band-6 mixer. The normal operating point is at the second minimum.

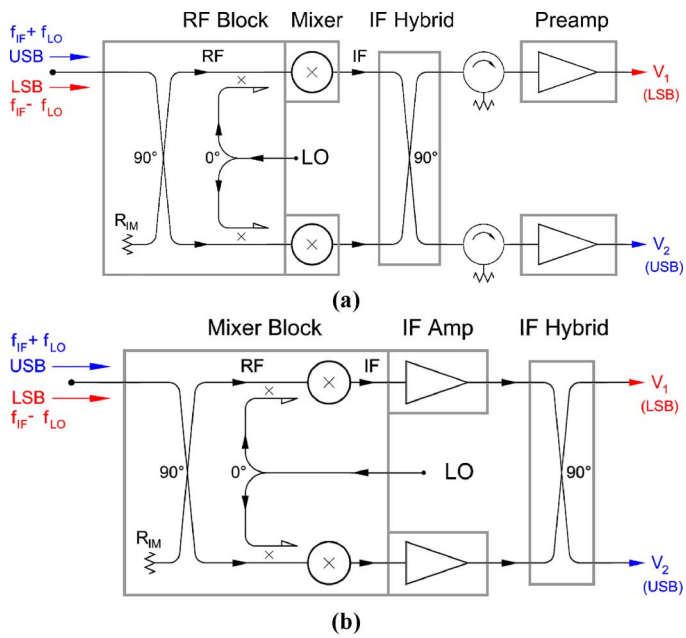


Fig. 16. Sideband-separating mixer-preamplifier configurations. (a) For Band 3, the elemental DSB mixer chips are in separate modules attached to the RF block containing the RF hybrid and LO couplers. The IF hybrid follows the mixers and the IF amplifiers are preceded by isolators. (b) For Band 6, the IF preamplifiers are attached directly to the block containing the elemental DSB mixers, RF hybrid, and LO couplers, and the IF hybrid follows the amplifiers. IF isolators are not used. For both bands, $R_{IM}$ is the image termination on the fourth port of the RF hybrid.

(single electrons from broken Cooper pairs) [25]. It is the quasi-particle current–voltage characteristic, whose strong non-linearity is seen in Figs. 6 and 7, which is used in SIS mixers. The Cooper pair current, or Josephson current, has a complex nonlinearity which can be characterized as a voltage-controlled oscillator [35] connected in parallel with the quasi-particle circuit. The presence of the Josephson effect in an SIS mixer can seriously degrade the noise temperature [36], but fortunately the Josephson current can be suppressed by a magnetic field applied between the electrodes of an SIS junction, and many SIS mixers include a solenoid with pole pieces which concentrate a magnetic field in the vicinity of the junctions. For the Band-6 mixers, a field of $\sim$ 180 Gauss is produced by a current of $\sim$ 26 mA in a coil of 5500 turns of superconducting wire. The magnet

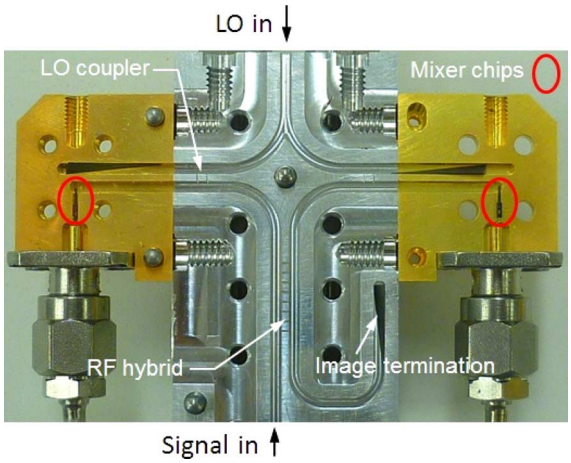


Fig. 17. One half of the Band-3 mixer assembly. The central aluminum block contains the waveguide branch-line hybrid, LO power divider, LO couplers, and the image termination. The DSB mixer chips and LO terminations are in the left and right modules. The RF signal enters through the lower waveguide and the LO power through the upper waveguide.

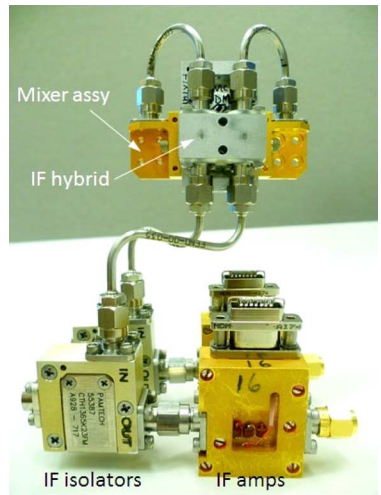


Fig. 18. Band-3 front-end. The mixer assembly is at the top, behind the IF quadrature hybrid (aluminum). Below them are the IF isolators and preamplifiers.

circuit is made of Consumet magnet iron and is similar to the one described in [37]. Fig. 15 shows the dependence of the critical current on magnet current for the two SIS chips in a typical Band-6 mixer. In Band 3, a magnetic field is not currently used. The general experience in radio astronomy is that a magnet is not required for lower frequency SIS receivers. However, it has recently been found that, on ALMA, with its very stringent stability requirements, the Band-3 receivers do need a magnetic field for the most sensitive observations; this is planned as a future upgrade.

## III. Sideband-Separating Mixers

For Band 6 (211–275 GHz), the complete sideband-separating mixer [38] consists of an E-plane split-block waveguide assembly containing the elemental DSB mixer chips, branch-line waveguide hybrid [15], LO couplers [39], and 4-K image termination [40], attached directly to two 4–12-GHz IF preamplifiers [41] without IF isolators. For Band 3 (84–116 GHz), the elemental DSB mixer chips [8] are mounted in separate modules which are attached to a split-block waveguide assembly containing the branch-line waveguide hybrid and LO couplers [42] and external 4–8-GHz cryogenic IF isolators are used. Fig. 16(a) and (b) shows the configuration of the Band-3 and -6 mixers. An important component is the load $R_{IM}$ on the fourth port of the RF hybrid [40]. This is the image termination, whose thermal noise in the upper and lower sidebands is downconverted to, respectively, the lower and upper sideband IF outputs of the sideband-separating mixer. By including $R_{IM}$ in the cryogenic mixer assembly, its contribution to the mixer noise temperature is minimized.

The amplitude and phase balance of the cryogenic IF quadrature hybrid is important in ensuring good image rejection. The initial Band-6 receivers used commercial IF hybrids which were found to be inconsistent at 4 K. Subsequently a cryogenic hybrid based on a design by Malo and Gallego [43] was implemented by MAC Technology [44] and has given excellent results.

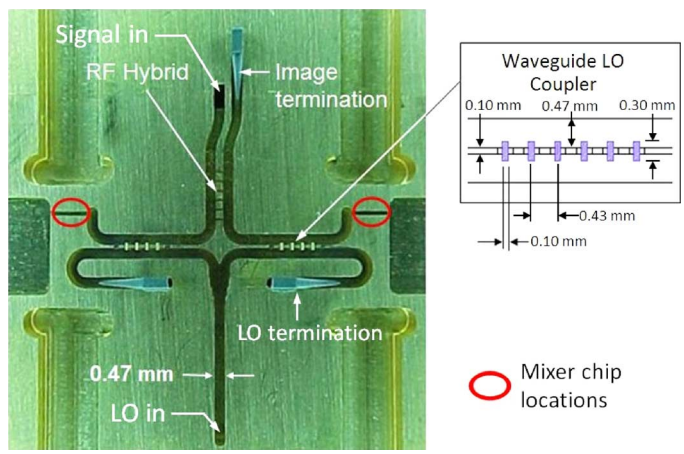


Fig. 19. One half of the Band-6 mixer, including the waveguide branch-line hybrid, LO power divider and LO couplers with their fourth-port terminations, the DSB mixer chips, and the image termination. The RF signal enters through a waveguide perpendicular to the page in the upper part of the circuit [28] and the LO enters through a similar waveguide in the lower part of the mating half of the block.

For the Band-6 mixers, the IF preamplifiers are selected to have well matched gain and phase *vs* frequency at 4 K; this is necessary because the preamplifiers are located in the signal path before separation of the sidebands in the IF hybrid. The amplifiers were selected in pairs with gain and phase differences which would result in no less than 17-dB image rejection (see [15, Fig. 2]). For the Band-3 configuration, gain and phase matching of the preamps is not necessary because they are after the IF hybrid, but isolators are necessary to ensure that reflection of the IF signal at the amplifier inputs does not degrade the image rejection.

Fig. 17 shows the Band-3 mixer assembly with the lids removed, and Fig. 18 shows the Band-3 mixer connected to the IF hybrid, IF isolators, and preamplifiers. Fig. 19 shows the Band-6 mixer with the lid removed. It includes the branch-line waveguide RF hybrid, LO power divider and LO couplers with their fourth-port terminations, and the image termination. Fig. 20

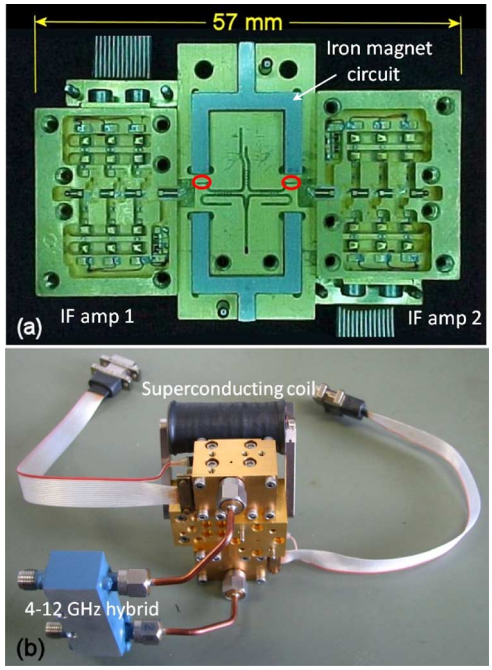


Fig. 20. Band-6 mixer assembly. (a) With preamps attached, lids removed. The red ellipses indicate the location of the mixer chips. (b) With IF hybrid and magnet circuit.

shows the Band-6 mixer-preamp assembly (a) with the mixer and amplifier lids removed and (b) with the IF hybrid and magnet circuit in place.

## IV. Measurement of the Mixers

The noise temperature and gain of the mixer-preamps were measured using room-temperature and liquid nitrogen loads placed in front of the vacuum window of a test Dewar. For sideband-separating receivers, it is possible to measure the image rejection accurately, without knowing the power level of the RF test signal, by using the procedure described in [45]. Knowing the image rejection, the SSB noise temperatures can be corrected to remove the contribution to the Y-factor from the image band (which acts to increase the Y-factor, thereby reducing the apparent SSB noise temperature). The mixer-preamp gain is determined from the change in IF output power of the test receiver when RF hot and cold loads with known temperatures are placed in front of the receiver, knowing the gain and noise temperature of the subsequent IF stages. For Band 3, the measured mixer-preamp SSB noise temperature, gain, and image rejection are shown in Fig. 21 for superior and typical mixer-preamps. The LO was tuned in 4-GHz increments, and at each LO frequency the mixer-preamp was measured across the IF band in 100-MHz steps. Similar results for Band 6 are shown in Fig. 22. The results in Figs. 21 and 22 include the contributions of the RF (quasi-optical) vacuum window, infrared filter, and cold optics in the Dewar and are corrected for the finite image rejection to give true SSB numbers.

## V. Discussion

The receiver noise temperatures shown in Figs. 21 and 22 are consistent with the analysis of the elemental DSB SIS mixers in Section II-A which is based on the measured $I(V)$ characteristics. The approximate noise contributions of the components ahead of the Band-3 and -6 mixer-preamps are shown in Tables I and II, calculated from the loss and physical temperature of each component. In the tables, the "$T_N$" column gives the effective input noise temperature $T_N = T_{CW}(L-1)$ of each component using the Callen and Welton radiation law (which is equivalent to the Planck law plus the zero-point fluctuation noise [46], [47]). The "$T_R$" column shows the receiver noise temperature which would be measured looking into the receiver at each component. The "image termination noise" is the contribution of the image termination resistor, $R_{IM}$ in Figs. 1 and 16, also calculated using the Callen and Welton law (which is why the component $T_N$ is greater than the physical temperature). The "LO coupled noise" is the sideband noise from the LO, and depends on the LO source.

TABLE I
Band-3 Noise Analysis

| BAND 3 | L dB | $T_{PHYS}$ K | $T_N$ K | $T_R$ K | Ref. |
|---|---|---|---|---|---|
| Window | 0.02 | 298 | 1.4 | 27.0 | [48] |
| I/R filter | 0.01 | 77 | 0.2 | 25.5 | |
| Horn + OMT | 0.37 | 4.2 | 0.4 | 25.3 | [49][50] |
| Waveguide | 0.03 | 4.2 | 0.0 | 22.8 | [49][50] |
| Image term. noise | | 4.2 | 4.6 | 22.6 | |
| LO Coupled noise | | | 3.0 | 18.0 | |
| Mixer-Preamp | | | 15.0 | 15.0 | |

TABLE II
Band-6 Noise Analysis

| BAND 6 | L dB | $T_{PHYS}$ K | $T_N$ K | $T_R$ K | Ref. |
|---|---|---|---|---|---|
| Window | 0.04 | 298 | 2.8 | 44.4 | [51] |
| I/R filter | 0.02 | 77 | 0.4 | 41.2 | |
| Horn + OMT | 0.20 | 4.2 | 0.3 | 40.7 | [49][50] |
| Waveguide | 0.30 | 4.2 | 0.5 | 38.6 | [49][50] |
| Image term. noise | | 4.2 | 6.6 | 35.6 | |
| LO Coupled noise | | | 3.0 | 29.0 | |
| Mixer-Preamp | | | 15.0 | 26.0 | |

During testing of some Band-6 mixer-preamps, a very weak spurious signal was occasionally detected near 230 GHz. This was eventually traced to oscillation at 230 GHz within one of the discrete InP HFET chips in the IF amplifiers. The 230-GHz signal leaked through the RF choke into the SIS mixer where it was down-converted to IF. This was cured by adjusting the drain bias or replacing the transistor.

At millimeter wavelengths, calibration of the individual sideband sensitivities of a DSB receiver is difficult and usually impractical on the telescope. The upper and lower sideband sensitivities can differ by several decibels, particularly at the extremes of the tuning range. A benefit of the sideband-separating receiver is the simplicity of calibrating the sensitivities of the upper and lower sidebands using the procedure mentioned in Section IV.

A problem well known to radio astronomers is the presence of variations, or ripples, in the baseline of a measured spectrum which make it difficult to identify weak spectral features in the source. These baseline ripples are caused by the standing wave between an imperfectly matched receiver input and the telescope optics. The standing wave pattern changes slightly during a long integration due to dimensional changes in the

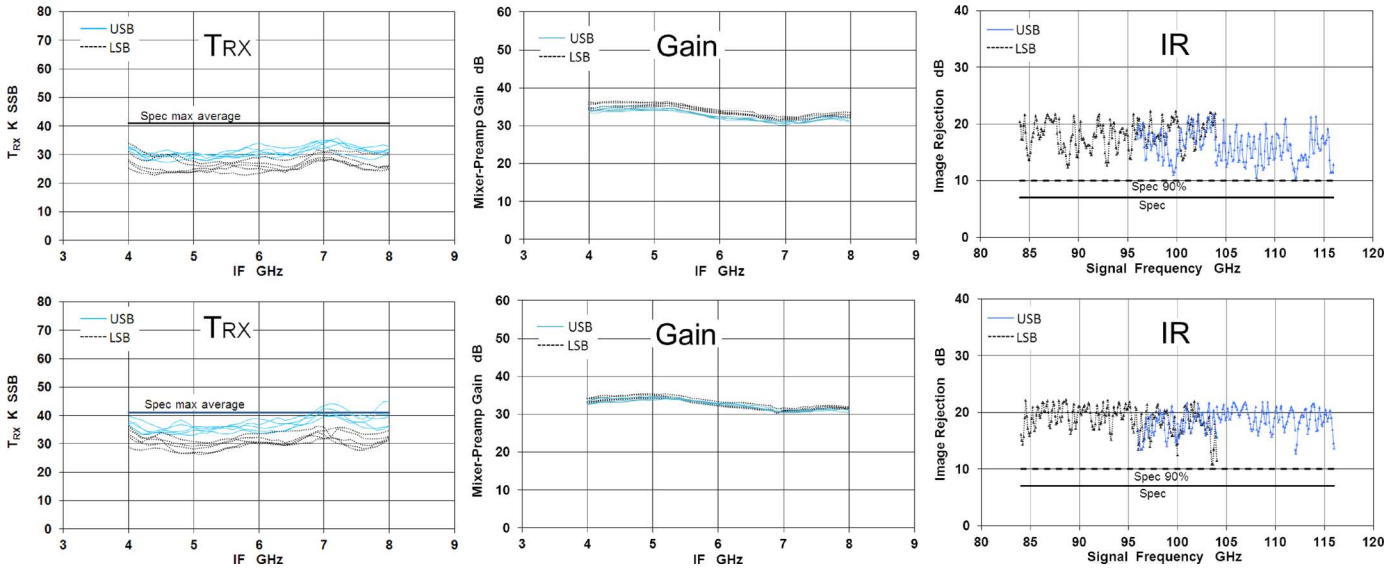


Fig. 21. Measured SSB noise temperature, gain, and image rejection, for two Band-3 mixer-preamps. The upper and lower plots are for superior and typical units, respectively. The LO was stepped from 92 to 108 GHz in 4-GHz increments at each of which the mixers were measured from 4 to 8 GHz IF in 100-MHz increments. The line labeled "Spec max average" indicates the specified maximum noise temperature measured in a 4-GHz IF bandwidth and averaged over both upper and lower sidebands in both polarization channels.

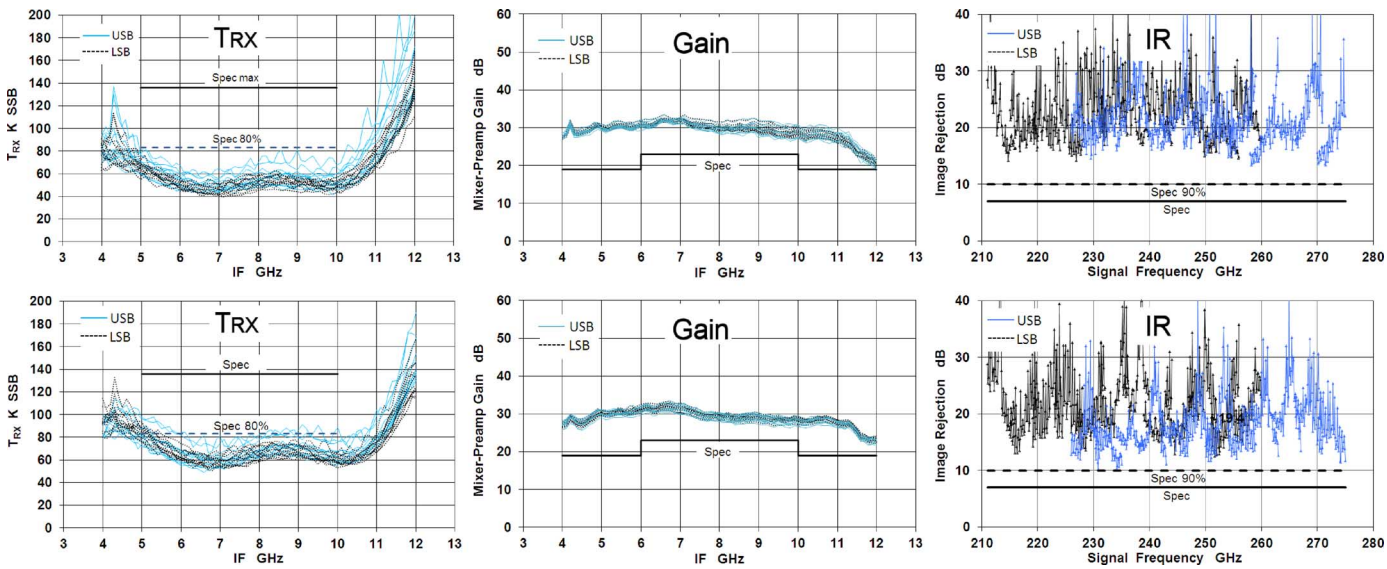


Fig. 22. Measured SSB noise temperature, gain, and image rejection, for two Band-6 mixer-preamps. The upper and lower plots are for superior and typical units, respectively. The LO was stepped from 221 to 265 GHz in 4-GHz increments at each of which the mixers were measured from 4 to 12 GHz IF in 100-MHz increments. The line labeled "Spec max" is the specified maximum noise temperature, and the line "Spec 80%" is the specified maximum noise temperature over at least 80% of the band.

telescope. This problem can be particularly severe in a receiver with a poorly matched input, which is characteristic of most DSB mixer receivers. It has been noted [52] that sideband-separating mixers described here have excellent spectral baseline stability compared with the usual DSB receivers. We believe this is a result of the RF quadrature hybrid at the input of the sideband-separating receiver. As in the case of a balanced amplifier [53], the circuit is inherently well matched, with the return loss limited only by the phase and amplitude imbalance of the hybrid and the difference between the RF input impedances of the elemental DSB mixers.

## VI. Conclusion

A total of 146 Band-3 sideband-separating mixers have been built and tested at NRC-Canada and delivered to ALMA in 73 dual-polarized cartridges. During the 2003–2009 production period, cryogenic tests were done on 515 Band-3 DSB mixer modules and 293 sideband-separating mixer assemblies. For Band 6, a total of 158 sideband-separating mixer-preamps have been built and tested at NRAO and delivered to ALMA, 146 in 73 dual-polarized cartridges and 12 spare units. During the 2008–2012 production period, cryogenic tests were done on 780 Band-6 mixer-preamps.

The SIS mixer chips for Bands 3 and 6 were all made at the University of Virginia Microfabrication Laboratory.

As ALMA nears completion, six of the ten bands use sideband-separating SIS mixers similar in varying degrees to those described here. The Band-4, -5, -7, and -8 mixers are described in [54]–[57]. Multibeam sideband-separating SIS receivers have also been developed for use on single-dish telescopes, as described in [58] and [59].

## ACKNOWLEDGMENT

The authors gratefully acknowledge the substantial contributions of the following to the fabrication and testing of the Band-3 and -6 mixer preamps: E. Bryerton, D. Derdall, D. Erickson, D. Garcia, R. Groves, N. Horner, F. Johnson, M. Lambeth, T. Marshall, M. Morgan, G. Morris, G. Petencin, M. Pospieszalski, G. Rodrigues, K. Saini, D. Schmitt, K. Yeung, and J.-Z. Zhang. The authors would also like to thank C. Cunningham and J. Webber for their enlightened management of the ALMA-North America front-end development and production. ALMA is a partnership of ESO (representing its member states), NSF (USA) and NINS (Japan), together with NRC (Canada) and NSC and ASIAA (Taiwan), in cooperation with the Republic of Chile. The Joint ALMA Observatory is operated by ESO, AUI/NRAO and NAOJ.

## REFERENCES

[1] P. L. Richards, T. M. Shen, R. E. Harris, and F. L. Lloyd, "Quasiparticle heterodyne mixing in SIS tunnel junctions," *Appl. Phys. Lett.*, vol. 34, no. 5, pp. 345–347, Mar. 1979.

[2] G. J. Dolan, T. G. Phillips, and D. P. Woody, "Low-noise 115-GHz mixing in superconducting oxide-barrier tunnel junctions," *Appl. Phys. Lett.*, vol. 34, no. 5, pp. 347–349, Mar. 1979.

[3] S. Rudner and T. Claeson, "Arrays of superconducting tunnel junctions as low noise 10-GHz mixers," *Appl. Phys. Lett.*, vol. 34, no. 10, pp. 711–713, May 1979.

[4] S.-K. Pan, M. J. Feldman, A. R. Kerr, and P. Timbie, "Low-noise 115-GHz receiver using superconducting tunnel junctions," *Appl. Phys. Lett.*, vol. 43, no. 8, pp. 786–788, Oct. 1983.

[5] A. Wootten and A. R. Thompson, "The Atacama large millimeter/submillimeter array," *Proc. IEEE*, vol. 97, no. 8, pp. 1463–1471, Aug. 2009.

[6] R. Blundell, C.-Y. E. Tong, D. C. Papa, R. L. Leombruno, X. Zhang, S. Paine, J. Stern, H. G. LeDuc, and B. Bumble, "A wideband fixed-tuned SIS receiver for 200 GHz operation," *IEEE Trans. Microw. Theory Techn.*, vol. MTT-43, no. 4, pp. 933–937, Apr. 1995.

[7] A. R. Kerr, S.-K. Pan, A. W. Lichtenberger, and H. H. Huang, "A Tunerless SIS mixer for 200–280 GHz with low output capacitance and inductance," in *Proc. 9th Int. Symp. Space Terahertz Technol.*, Mar. 17–19, 1998, pp. 195–203.

[8] S.-K. Pan, A. R. Kerr, M. W. Pospieszalski, E. F. Lauria, W. K. Crady, N. Horner Jr., S. Srikanth, E. Bryerton, K. Saini, S. M. X. Claude, C. C. Chin, P. Dindo, G. Rodrigues, D. Derdall, J. Z. Zhang, and A. W. Lichtenberger, "A fixed-tuned SIS mixer with ultra-wide-band IF and quantum-limited sensitivity for ALMA Band 3 (84–116 GHz) receivers," in *Proc. 15th Int. Symp. Space Terahertz Technol.*, Northampton, MA, USA, Apr. 27–29, 2004, pp. 62–69.

[9] N. R. Erickson, "A very low-noise single-sideband receiver for 200–260 GHz," *IEEE Trans. Microw. Theory Techn.*, vol. MTT-33, no. 11, pp. 1179–1188, Nov. 1985.

[10] J. M. Payne, "Millimeter and submillimeter wavelength radio astronomy," *Proc. IEEE*, vol. 77, no. 7, pp. 993–1017, Jul. 1989.

[11] J. M. Payne, J. W. Lamb, J. G. Cochran, and N. Bailey, "A new generation of SIS receivers for millimeter-wave radio astronomy," *Proc. IEEE*, vol. 82, no. 5, pp. 811–823, May 1994.

[12] A. R. Kerr, "Image frequency suppression on the MMA," National Radio Astronomy Observatory, Charlottesville, VA, Millimeter Array Memo #70, 1991.

[13] A. R. Kerr and S.-K. Pan, "Design of planar image-separating and balanced SIS mixers," in *Proc. 7th Int. Symp. Space Terahertz Technol.*, Mar. 12–14, 1996, pp. 207–219.

[14] A. R. Kerr, S.-K. Pan, and H. G. LeDuc, "An integrated sideband separating SIS mixer for 200–280 GHz," in *Proc. 9th Int. Symp. Space Terahertz Technol.*, Mar. 17–19, 1998, pp. 215–221.

[15] S. M. X. Claude, C. T. Cunningham, A. R. Kerr, and S.-K. Pan, "Design of a sideband-separating balanced SIS mixer based on waveguide hybrids, ALMA Memo No. 316, 2000.

[16] J. R. Tucker, "The quantum response of nonlinear tunnel junction as detectors and mixers," in *Reviews of Infrared & Millimeter Waves*. New York, NY, USA: Plenum, 1983, vol. 1, pp. 47–75.

[17] J. R. Tucker and M. J. Feldman, "Quantum detection at millimeter wavelengths," *Rev. Mod. Phys.*, vol. 57, no. 4, pp. 1055–1113, Oct. 1985.

[18] Q. Ke and M. J. Feldman, "Optimum source conductance for high frequency superconducting quasiparticle receivers," *IEEE Trans. Microw. Theory Techn.*, vol. 41, no. 4, pp. 600–604, Apr. 1993.

[19] J. D. Kraus, *Radio Astronomy*, 2nd ed. Powell, OH, USA: Cygnus-Quasar, 1986.

[20] A. R. Kerr, "Some fundamental and practical limits on broadband matching to capacitive devices, and the implications for SIS mixer design," *IEEE Trans. Microw. Theory Techn.*, vol. MTT-43, no. 1, pp. 2–13, Jan. 1995.

[21] A. R. Kerr, S.-K. Pan, and S. Withington, "Embedding impedance approximations in the analysis of SIS mixers," *IEEE Trans. Microw. Theory Techn.*, vol. 41, no. 4, pp. 590–594, Apr. 1993.

[22] M. J. Feldman, S.-K. Pan, and A. R. Kerr, "Saturation of the SIS mixer," in *Int. Superconductivity Electron. Conf. Dig. Tech. Papers*, Tokyo, Aug. 1987, pp. 290–292.

[23] A. R. Kerr, "Saturation by noise and CW signals in SIS mixers," in *Proc. 13th Int. Symp. Space Terahertz Technol.*, Mar. 26–28, 2002, pp. 11–22.

[24] M. J. Feldman and S. Rudner, "Mixing with SIS arrays," in *Reviews of Infrared & Millimeter Waves*. New York, NY, USA: Plenum, 1983, vol. 1, pp. 47–75.

[25] T. van Duzer and C. W. Turner, *Principles of Superconductive Devices and Circuits*, 2nd ed. New York, NY, USA: Prentice-Hall, 1999.

[26] D. M. Lea, A. W. Lichtenberger, A. R. Kerr, S.-K. Pan, and R. F. Bradley, "On-wafer resonant structures for penetration depth and specific capacitance measurements of Nb/Al-Al2O3/Nb trilayer films," Appl. Supercond. Conf., 1994, unpublished poster.

[27] W. Clark, J. Z. Zhang, and A. W. Lichtenberger, "Ti quadlevel resist process for the fabrication of Nb SIS junctions," *IEEE Trans. Appl. Superconduct.*, vol. 13, pp. 115–118, 2003.

[28] A. R. Kerr, "Elements for E-plane split-block waveguide circuits," ALMA Memo 381, 2001.

[29] Sonnet *em* Simulator. Sonnet Software, Syracuse, NY, USA.

[30] A. R. Kerr, "Surface impedance of superconductors and normal conductors in EM simulators," Nat. Radio Astron. Observatory, Charlottesville, VA, USA, Millimeter Array Memo 245, 1999.

[31] MMICADv2. Optotek, Ontario, Canada.

[32] S.-K. Pan, A. R. Kerr, M. J. Feldman, A. Kleinsasser, J. Stasiak, R. L. Sandstrom, and W. J. Gallagher, "A 85–116 GHz SIS receiver using inductively shunted edge-junctions," *IEEE Trans. Microw. Theory Techn.*, vol. MTT-37, no. 3, pp. 580–592, Mar. 1989.

[33] Model CTH1365K23FM. Pamtech Inc. [Online]. Available: http://pamtechinc.com

[34] Part MSI-210-0518-XX. Mini-Systems Inc., Attleboro, MA, USA.

[35] C. A. Hamilton, "Analog simulation of a Josephson junction," *Rev. Sci. Instrum.*, vol. 43, no. 3, pp. 445–447, Mar. 1972.

[36] M. J. Wengler, N. B. Dubash, G. Pance, and R. E. Miller, "Josephson effect gain and noise in SIS mixers," *IEEE Trans Microw. Theory Techn.*, vol. 40, no. 5, pp. 820–826, May 1992.

[37] G. A. Ediss and K. Crady, "Measurements of materials for SIS mixer magnetic circuits," Nat. Radio Astron. Observatory, Charlottesville, VA, USA, ALMA Memo 438, 2002.

[38] A. R. Kerr, S.-K. Pan, E. F. Lauria, A. W. Lichtenberger, J. Zhang, M. W. Pospieszalski, N. Horner, G. A. Ediss, J. E. Effland, and R. L. Groves, "The ALMA band 6 (211–275 GHz) sideband-separating SIS mixer-preamplifier," in *Proc. 15th Int. Symp. Space THz Tech.*, Northampton, MA, USA, Apr. 2004, pp. 55–61.

[39] A. R. Kerr and N. Horner, "A split-block waveguide directional coupler," Nat. Radio Astron. Observatory, Charlottesville, VA, USA, ALMA Memo 432, 2002.

[40] A. R. Kerr, H. Moseley, E. Wollack, W. Grammer, G. Reiland, R. Henry, and K. P. Stewart, MF-112 and MF-116: Compact Waveguide Loads and FTS Measurements at Room Temperature and 5 K National Radio Astronomy Observatory, Charlottesville, VA, 2004, ALMA Memo 494.

[41] E. F. Lauria, A. R. Kerr, M. W. Pospieszalski, S.-K. Pan, J. E. Effland, and A. W. Lichtenberger, "A 200–300 GHz SIS mixer- preamplifier with 8 GHz IF bandwidth," in *IEEE MTT-S Int. Microw. Symp. Dig.*, May 2001, pp. 1645–1648.

[42] P. Dindo, S. Claude, D. Derdall, D. Henke, D. Erickson, G. Rodrigues, A. Lichtenberger, and S.-K. Pan, "Design and characterization of sideband-separating SIS mixer RF hybrids for the band 3 receiver (84–116 GHz)," in *Proc. Joint 30th Int. Conf. Infrared and Millimeter Waves and the 13th Int. Conf. on Terahertz Electron.*, Sep. 2005, pp. 409–410.

[43] I. Malo, J. D. Gallego, M. C. Diez, C. Cortes, and C. Briso, "Cryogenic hybrid coupler for ultra low noise radioastronomy receiver," in *IEEE MTT-S Int. Microw. Symp. Dig.*, 2009, pp. 1005–1008.

[44] Model CA7256D. MAC Technology Inc., Klamath Falls, OR, USA [Online]. Available: http://www.mactechnology.com

[45] A. R. Kerr, S.-K. Pan, and J. E. Effland, "Sideband calibration of millimeter-wave receivers," ALMA Memo 357, 2001.

[46] A. R. Kerr, "Suggestions for revised definitions of noise quantities, including quantum effects," *IEEE Trans. Microw. Theory Techn.*, vol. 47, no. 3, pp. 325–329, Mar. 1999.

[47] A. R. Kerr and J. Randa, "Thermal noise and noise measurements—A 2010 update," *IEEE Microw. Mag.*, vol. 11, no. 6, pp. 40–52, Oct. 2010.

[48] S. Claude, P. Dindo, D. Erickson, F. Jiang, K. Yeung, D. Derdall, D. Duncan, D. Garcia, D. Henke, B. Leckie, A. Lichtenberger, P. Niranjanan, S.-K. Pan, M. Pfleger, G. Rodrigues, K. Szeto, P. Welle, and K. Caputa, "The band 3 receiver (84–116 GHz) for ALMA," in *Proc. 30th Int. Conf. Infrared and Millimeter Waves*, Williamsburg, VA, USA, Sep. 19–23, 2005.

[49] A. R. Kerr, C. Litton, G. Petencin, D. Koller, and M. Shannon, "Loss of gold plated waveguides at 210–280 GHz," ALMA Memo 585, 2009.

[50] R. Finger and A. R. Kerr, "Microwave loss reduction in cryogenically cooled conductors," *Int. J. Infrared Millimeter Waves*, vol. 29, no. 10, pp. 924–932, Oct. 2008.

[51] D. Koller, A. R. Kerr, and G. A. Ediss, "Proposed quartz vacuum window designs for ALMA Bands 3–10," ALMA Memo 397, 2001.

[52] E. F. Lauria, A. R. Kerr, G. Reiland, R. F. Freund, A. W. Lichtenberger, L. M. Ziurys, M. Metcalf, and D. Forbes, "First astronomical observations with an ALMA Band 6 (211–275 GHz) sideband-separating SIS mixer-preamp," ALMA Memo 553, 2006.

[53] R. S. Engelbrecht and K. Kurokawa, "A wideband low noise L-band balanced transistor amplifier," *Proc. IEEE*, vol. 53, no. 3, pp. 237–247, Mar. 1965.

[54] S. Asayama, S. Kawashima, H. Iwashita, T. Takahashi, M. Inata, Y. Obuchi, T. Suzuki, and T. Wada, "Design and development of ALMA band 4 cartridge receiver," in *Proc. 19th Int. Symp. Space Terahertz Technol.*, Groningen, Germany, Apr. 2008, pp. 244–249.

[55] B. Billade, O. Nystrom, D. Meledin, E. Sundin, I. Lapkin, M. Fredrixon, V. Desmaris, H. Rashid, M. Strandberg, S. Ferm, A. Pavolotsky, and V. Belitsky, "Performance of the first ALMA band 5 production cartridge," *IEEE Trans. THz Sci. Technol.*, vol. 2, no. 1, pp. 208–214, Jan. 2012.

[56] S. Mahieu, D. Maier, B. Lazareff, A. Navarrini, G. Celestin, J. Chalain, D. Geoffroy, F. Laslaz, and G. Perrin, "The ALMA band-7 cartridge," *IEEE Trans. THz Sci. Technol.*, vol. 2, no. 1, pp. 29–39, Jan. 2012.

[57] Y. Sekimoto, Y. Iizuka, N. Satou, T. Ito, K. Kumagai, M. Kamikura, M. Naruse, and W. L. Shan, "Development of ALMA band 8 (385–500 GHz) cartridge," in *Proc. 19th Int. Symp. Space Terahertz Technol.*, Groningen, Germany, Apr. 2008, pp. 253–257.

[58] T. Nakajima, K. Kimura, T. Katase, M. Koyano, H. Inoue, T. Sakai, H. Iwashita, C. Miyazawa, S. Asayama, N. Kuno, H. Ogawa, T. Onishi, R. Kawabe, and T. Noguchi, "Development of a new multi-beam array 2SB receiver in 100 GHz band for the NRO 45-m radio telescope," in *Proc. Int. Symp. Space Terahertz Technol.*, Tokyo, Japan, Apr. 2012, pp. 12.1–12.4.

[59] W. Shan, J. Yang, S. Shim, Q. Yao, Y. Zuo, Z. Lin, S. Chen, X. Zhang, W. Duan, A. Cao, S. Li, Z. Li, J. Liu, and J. Zhong, "Development of superconducting spectroscopic array receiver: A multibeam 2SB SIS receiver for millimeter-wave radio astronomy," *IEEE Trans. THz Sci. Technol.*, vol. 2, no. 6, Nov. 2012.

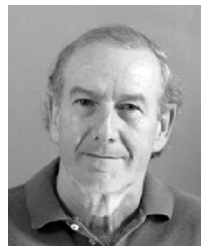

**Anthony R. Kerr** (S'64–A'66–SM'78–F'84–LF'08) received the Ph.D. degree from the University of Melbourne, Melbourne, Australia, in 1969.

He then joined the Commonwealth Scientific and Industrial Research Organization, Sydney, Australia, to develop cryogenic parametric amplifiers for radio astronomy. From 1971 to 1974, he worked at the National Radio Astronomy Observatory, Charlottesville, VA, USA, developing the first cryogenically cooled Schottky-diode mixer receiver for millimeter wavelength radio astronomy. Between 1974 and 1984, at the NASA/Goddard Institute for Space Studies, New York, he worked on the theory and design of Schottky, Josephson, and SIS mixers for millimeter-wave receivers. In 1984, he returned to the National Radio Astronomy Observatory, where he is responsible for development of low-noise millimeter- and submillimeter-wave receiver technology.

Dr. Kerr was corecipient of the 1978 IEEE Microwave Prize and in 1983 was the recipient of the NASA Exceptional Engineering Achievement Medal.

**Shing-Kuo Pan** (S'81–M'85) was born in Taiwan in 1953. He received the B.A. degree from Fu-Jen University, New Taipei City, Taiwan, in 1976, and the M.A., M.Phil., and Ph.D. degrees in physics from Columbia University, New York, NY, USA, in 1980, 1981 and 1984, respectively.

Since 1984, he has been with the National Radio Astronomy Observatory, Charlottesville, VA, USA, where he has been involved in research on SIS detectors and in the development of SIS heterodyne receivers for radio astronomy. He is responsible for the development of the Band 3 SIS mixer for the Atacama Large Millimeter Array (ALMA) project, currently under construction by an international partnership between countries in North America (United States and Canada), Europe, and East Asia. He also supports the SIS receiver on the Harvard-Smithsonian Sky Survey radio telescope at Cambridge, MA. His other interests include computer-aided design, superconducting device fabrication techniques, and noise mechanisms in superconducting devices.

Dr. Pan is a member of the American Physical Society.

**Stéphane M. X. Claude** received the engineering degree in material sciences from the Ecole Nationale Supérieure d'Ingénieurs de Caen, Caen, France, in 1990, and the Ph.D. degree in physics from London University, Queen Mary and Westfield College, London, U.K., in 1996.

From 1990 to 1996, he was a Research Associate with the Rutherford Appleton Laboratory, U.K., where he developed techniques for the fabrication of superconducting–insulator–superconducting (SIS) mixer chips, for low-noise submillimetre receivers in radio astronomy. Part of his Ph.D. work was to commission a 500-GHz receiver at the James Clerk Maxwell Telescope (JCMT) in Hawaii. In 1996, he joined the Herzberg Institute of Astrophysics, Victoria, BC, Canada, where he continued development on low-noise receivers for astronomy, including a 200-GHz receiver for the JCMT and a sideband separating mixer design. From 2000 to 2002, he was with the Institut de Radioastronomie Millimétrique (IRAM), Grenoble, France, where he worked on the design of a 275–370-GHz receiver (Band 7) for the Atacama Large Millimetre Array (ALMA). Since 2002, he has been leading the millimeter instrumentation team at the Herzberg Institute of Astrophysics, National Research Council, Victoria, BC, Canada. He was a Project Engineer for the 84–116 GHz receiver (Band 3) developed for the ALMA. He was an Adjunct Professor with the Ecole Polytechnique de Montréal, Montréal, QC, Canada, for the period 2006–2010. Since 2003, he has been an Adjunct Associate Professor with the University of Victoria, Victoria, BC, Canada.

His research interests include millimeter-wave low-noise receivers and phased array feeds for radio astronomy.

**Philip Dindo** received the B.S. and M.S. degrees from University of British Columbia, Victoria, BC, Canada, in 1982 and 1985, respectively, and the Ph.D. degree from the University of Ottawa, Ottawa, ON, Canada, in 1994, all in electrical engineering.

Since 1985, he worked in various RF and optical industries, including Optotek Limited and JDS Fitel Inc., Ottawa, ON, Canada, fSona Optical Wireless, and National Research Council of Canada, Richmond, BC, Canada. His work interests are in the area of RF instrumentation and development of test sets control systems.

**Arthur W. Lichtenberger** received the B.A. degree in physics from Amherst College, Amherst, MA, USA, in 1980, and the M.S. and Ph.D. degrees in electrical engineering from the University of Virginia, Charlottesville, VA, USA, in 1985 and 1987, respectively.

In 1987, he joined the faculty of the University of Virginia, Charlottesville, VA, USA, where he is currently a Research Professor with the Department of Electrical and Computer Engineering and Director of the University of Virginia Microfabrication Laboratories. His current research interests include superconducting materials, devices and circuits in conjunction with submillimeter electronics, high-frequency instrumentation, and metrology.

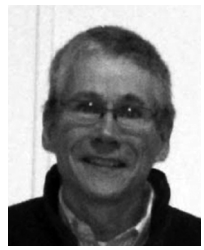

**John E. Effland** (S'78–M'81) received the B.S.E.E. degree from the University of Maryland, Baltimore, MD, USA, in 1979, and the M.S.E.E. degree in electrophysics from George Washington University, Washington, DC, USA, in 1982.

While at Comsat Laboratories, he built G/T measurement systems for 30-m class earth stations and was a member of a team that developed flat platform antennas for an early direct broadcast satellite system. While at Interferometrics, he was a member of a team that developed holography measurement systems, satellite interference location systems, and an interferometric satellite tracking system. He joined the National Radio Astronomy Observatory, Charlottesville, VA, USA, in 1998 and worked on SIS mixer measurement systems. He was then the Technical Manager for construction of ALMA Band-6 receivers and testing of ALMA front ends.

**Eugene F. Lauria** (M'94) received the B.S.E.C.E. and M.S.E.E. degrees from the University of Massachusetts, Amherst, MA, USA, in 1988 and 1992, respectively.

While at the University of Massachusetts, he was with the Five College Radio Observatory, where he studied Fourier optics and worked on millimeter-wave radio receivers for the Quabbin 14-meter radio telescope. After leaving University of Massachusetts in 1993, he joined the National Astronomy and Ionosphere Center Receiver Laboratory, Cornell University, Ithaca, NY, USA, and was responsible for the design and construction of the receiver frontends during the Gregorian Upgrade Project of Arecibo Observatory. In 1999, he joined the Central Development Laboratory, National Radio Astronomy Observatory, Charlottesville, VA, USA, and was involved in the development of the ALMA band-6 (211–275 GHz) cartridge. While there, he collaborated with the groups involved with ALMA band 3 (84–116 GHz) and band 9 (602–720 GHz) in cryogenic IF amplifier development. In 2005, he joined the engineering staff of the Arizona Radio Observatory where he is involved in millimeter and submillimeter receiver development for the Submillimeter Telescope on Mt. Graham and the Kitt Peak 12-m radio telescope